

# Kinetic Energy Driven Ferromagnetic Insulator

Jinyuan Ye,<sup>1,2,3</sup> Yuche He,<sup>4,\*</sup> and Congjun Wu<sup>2,3,5,6,†</sup>

<sup>1</sup>*Department of Physics, Fudan University, Shanghai, 200433, China*

<sup>2</sup>*New Cornerstone Science Laboratory, Department of Physics,*

*School of Science, Westlake University, Hangzhou 310024, Zhejiang, China*

<sup>3</sup>*Institute of Natural Sciences, Westlake Institute for Advanced Study, Hangzhou 310024, Zhejiang, China*

<sup>4</sup>*Rudolf Peierls Centre for Theoretical Physics, Clarendon Laboratory,  
Parks Road, Oxford OX1 3PU, United Kingdom*

<sup>5</sup>*Institute for Theoretical Sciences, Westlake University, Hangzhou 310024, Zhejiang, China*

<sup>6</sup>*Key Laboratory for Quantum Materials of Zhejiang Province,  
School of Science, Westlake University, Hangzhou 310024, Zhejiang, China*

We construct a minimal model of interacting fermions establishing a ferromagnetic insulating phase. It is based on the Hubbard model on a trimerized triangular lattice in the regime of  $U \gg t \gg |t'|$  with  $t > 0$  and  $t'$  the intra- and inter-trimer hopping amplitudes, respectively. At the  $\frac{1}{3}$ -filling, each trimer becomes a triplet spin-1 moment, and the inter-trimer superexchange is ferromagnetic with  $J = -\frac{2}{27} \frac{t'^2}{t}$  in the limit of  $U/t = +\infty$ . As  $U/t$  becomes finite, the antiferromagnetic superexchange competes with the ferromagnetic one. The system enters into a frustrated antiferromagnetic insulator when  $\lambda > U/t \gg 1$  where  $\lambda \sim 10$ . In contrast, a similar analysis performed on the trimerized Kagome lattice shows that only antiferromagnetic superexchange exists at  $1/3$ -filling.

The mechanism of ferromagnetism (FM) is a long-standing problem of strong correlation physics [1]. The driving force to itinerant FM is often thought to be the direct exchange among electrons with the same spin to reduce the inter-particle repulsion. Spin polarization pays a large cost of kinetic energy due to Pauli's exclusion principle, such that in most situations, fermions would rather develop unpolarized but highly correlated many-body ground states than be polarized. Nevertheless, a few rigorous results have been established: The Nagaoka theorem proves that the infinite  $U$  Hubbard model at half-filling with doping only a hole develops FM [2, 3], for bipartite lattice regardless of the sign of hopping, and for non-bipartite lattice with positive hopping. Another class of theorems of FM rely on the flat-band structure of line graphs in which the kinetic energy is suppressed to zero [4–7]. It is also shown that FM could remain stable under certain conditions even when the band structure becomes non-singular [8]. Furthermore, a series of theorems are proved that Hund's interaction combined with the quasi-1D band structure lead to itinerant FM in the multi-orbital Hubbard model over a large region of filling factors [9]. The Curie-Weiss metal state and the FM criticality are accurately studied by quantum Monte Carlo simulations free of the sign problem [10].

On the other hand, Mott insulators are typically dominated by antiferromagnetic (AFM) superexchange. Upon doping, they may serve as the parent compounds of high  $T_c$  superconductors. In frustrated systems, such as triangular and Kagome lattices, the AFM spin alignment of each bond can not be simultaneously realized due to geometry. An incredibly rich and complex nature of quantum magnetism manifests [11–15], leading to exotic states of spin liquid [16–18]. Owing to the

complexity of frustrated magnets, the cluster approach is also employed for theoretical studies. The cluster model extends beyond the concept of individual sites, focusing instead on well-defined clusters of atoms as the fundamental units. Unequal coupling strengths cause electrons to localize on these clusters, rather than on individual atomic sites. The localized degrees of freedom can be effectively described in terms of molecular orbitals, giving rise to what are often referred to as *molecules in solids* [19]. Coupled cluster can form cluster Mott insulators [20–22]. Experimentally, such clusters in triangular/Kagome lattices (trimers) have been observed in materials such as  $\text{LuFeO}_3$  [23], and the  $\text{Mo}_3\text{O}_8$  family of compounds [24–28]. Furthermore, the  $t$ - $t'$  triangular lattice here is expected to be achieved in cold-atom experiments [29–36].

It would be non-trivial to unify FM and AFM in the same system regarding to their different origins. In this article, we find the transition from a FM insulating state to the AFM one simply as varying interaction strengths. It is based on the Hubbard model defined in a trimerized triangular lattice at the  $1/3$ -filling in the strong correlation regime  $U \gg t \gg |t'|$ . Two electrons in each trimer form a spin-1 triplet at  $t > 0$ . The inter-trimer hopping generates both FM and AFM super exchanges, which involve intermediate excitations free of and with the double occupancy, respectively. A connection could be made to the non-trimerized case ( $t' = t$ ), where AFM dominates at half-filling and FM is believed to appear at finite hole/electron doping for positive/negative hopping with double occupancy suppressed by large  $U$  [37–43]. At  $U/t = \infty$ , the FM exchange dominates while it switches to the AFM one at a finite value around  $U/t \approx 13 \sim 15$ , as confirmed by the

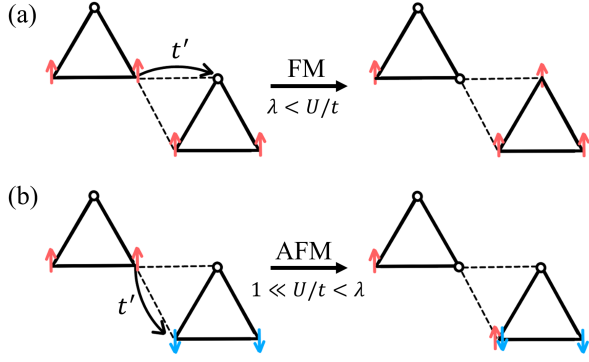


FIG. 1. Particle-hole excitations leading to (a) the FM superexchange at  $U/t > \lambda$  and (b) the AFM one at  $\lambda > U/t \gg 1$ , respectively. The transition value is about  $\lambda \sim 10$ . For the FM case, the excitation energy  $E_{ex} \sim t$  with only single occupations, while  $E_{ex} \sim U$  for the AFM case manifesting the Mott physics characterized by the double occupancy.

density-matrix-renormalization-group [44, 45] (DMRG) simulations. The FM insulating state remains robust by threading a weak staggered flux pattern of  $\phi$ , and it becomes a FM metal at small hopping levels. In contrast, as for the trimerized Kagome lattice, the inter-trimer exchange is always AFM-like. Our mechanism is different from the orbital-active Mott insulators in which FM exchange could appear according to the Kanamori-Goodenough rule. In that case, the overall nature remains anti-ferro, either ferro in orbital and antiferro in spin, or, antiferro in orbital and ferro in spin.

*Model Hamiltonian.*—We consider the Hubbard model  $H = H_0 + H'$  defined in a trimerized triangular lattice as illustrated in Fig. 2(a),

$$H_0 = t \sum_{\langle ij \rangle} \left\{ c_{i\sigma}^\dagger c_{j\sigma} + h.c. \right\} + U n_{i,\uparrow} n_{i,\downarrow},$$

$$H' = t' \sum_{\langle\langle ij' \rangle\rangle} \left\{ c_{i'\sigma}^\dagger c_{j'\sigma} + h.c. \right\}, \quad (1)$$

where  $H_0$  is the intra-trimer Hamiltonian, and  $H'$  describes the inter-trimer hoppings;  $\langle ij \rangle$  and  $\langle\langle ij' \rangle\rangle$  represent the intra- and inter-trimer bonds, respectively.  $t > 0$  is crucial for establishing FM below half-filling because the particle-hole symmetry is absent in the non-bipartite lattice. Two neighboring trimers are connected by two links, hence, the superexchanges between them is insensitive to the sign of  $t'$ .

The free band structure of the trimerized configuration is depicted in Fig. (S1) in Supplemental Material (SM.) (IA). Since  $t \gg |t'|$ , three intra-trimer states are solved as orbitals: the lower two are degenerate with the energy of  $E = -t$  and the upper with  $E = 2t$ . They are broadened into three bands whose widths are proportional to  $|t'|$ . The lower two bands overlap, and are separated from the upper one. The band gap  $\Delta_b$

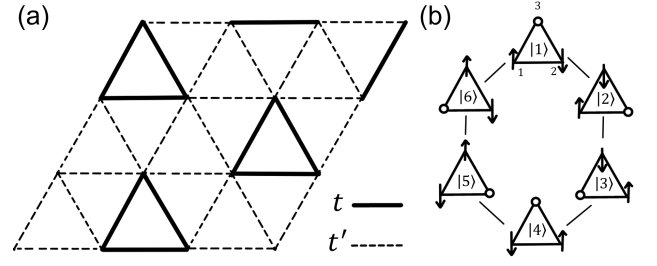


FIG. 2. (a) The trimerized triangular lattice with hopping strengths—the solid line represents the intra-trimer hopping  $t$  and the dashed one represents the inter-trimer hopping  $t'$ . Each trimer is filled with 2 electrons. (b) The bases of the sector with  $S_{tot} = 0$  are generated by the hole's hopping around the trimer, sequentially denoted as  $|1\rangle = c_{1\uparrow}^\dagger c_{2\downarrow}^\dagger |\Omega\rangle$ ,  $|2\rangle = c_{3\downarrow}^\dagger c_{1\uparrow}^\dagger |\Omega\rangle$ ,  $|3\rangle = c_{2\uparrow}^\dagger c_{3\downarrow}^\dagger |\Omega\rangle$ ,  $|4\rangle = c_{1\downarrow}^\dagger c_{2\uparrow}^\dagger |\Omega\rangle$ ,  $|5\rangle = c_{3\uparrow}^\dagger c_{1\downarrow}^\dagger |\Omega\rangle$ ,  $|6\rangle = c_{2\downarrow}^\dagger c_{3\uparrow}^\dagger |\Omega\rangle$ .

between them is at the order of  $t$  at  $|t'/t| \ll 1$ , while it closes at  $t'/t = 3/4$ .

Below we consider the filling of  $\frac{1}{3}$ , *i.e.*, 2 fermions per trimer. The lower two bands are effectively half-filled, hence, it should be metallic in the weak coupling regime of  $U/t' \sim 1$ . In contrast, the strong correlation regime is characterized by  $\min(U, t) \gg t'$ , and correlated insulating states appear. The inter-trimer hopping generates virtual excitations involving 1 or 3 fermions in a trimer. The dependence of  $E_{ex}$  on  $t$  and  $U$  here are depicted in Figs. 1(a) and 1(b), respectively, and are calculated in SM. (IB). Excitations with  $E_{ex} \sim t$  lead to the FM superexchange in the regime of  $U \gg t \gg t'$ . As lowering the value of  $U/t$ , the AFM superexchange becomes dominant as in the usual Mott insulators, and the excitations are characterized by double occupancy with  $E_{ex} \sim U$ . The evolution from the FM to AMF superexchange is explained below.

We begin with the case of  $U/t = +\infty$  which forbids the double occupancy. The Nagaoka theorem applies to the case with only a single hole in the entire system [2]. Below the dominance of the FM exchange is shown to occur at the  $\frac{1}{3}$ -filling.

*Single trimer.*—At  $t' = 0$  the system is reduced to disconnected trimers. When the trimer is filled with 2 electrons, it is sufficient to consider the sector of  $S_{tot,z} = 0$  within a trimer based on the SU(2) symmetry. This local Hilbert space contains 6 bases denoted as  $|m\rangle$  ( $m = 1 \sim 6$ ):  $|1\rangle = c_{1\uparrow}^\dagger c_{2\downarrow}^\dagger |\Omega\rangle$  with  $|\Omega\rangle$  denoting the vacuum state, and the other states  $|m\rangle$  are generated as the hole hops around the trimer in a clockwise way as shown in Fig. 2(b). In this convention,  $|m\rangle$  and  $|m+3\rangle$  correspond to a pair of states by flipping two spins. Applying  $H_0$  on  $|m\rangle$ , it yields  $H_0|m\rangle = -t(|m-1\rangle + |m+1\rangle)$ , where  $m$  is defined modulo 6.

Remarkably, this intra-trimer 2-electron problem exhibits a 6-fold rotational symmetry. This can be

mapped to a rolling motion problem: The pair of spin represents a 2-teeth external gear, and the trimer behaves as a 3-teeth internal gear. Since rolling is a combination of translation and rotation, one round is insufficient to restore the configurations of both degrees of freedom back to the initial ones. Instead, the minimal requirement to a periodicity requires rolling two rounds. Consequently, this problem is mapped to a single-body problem moving around a hexagon. It is interesting that the effective orbital angular momentum here is modulo 6 instead of 3, exhibiting a fractionalization behavior.

The eigenstates for the single trimer problem in the sector of  $S_{\text{tot},z} = 0$  are solved as  $|k_n\rangle = \frac{1}{\sqrt{6}} \sum_n e^{ik_n m} |m\rangle$  with the energy spectrum,

$$E_n = -2t \cos k_n, \quad (2)$$

where  $k_n = \frac{n}{3}\pi$  with  $n = 0, \pm 1, \pm 2, 3$ . The states with  $n = 0, \pm 2$  are symmetric under the operation  $m \rightarrow m+3$ , hence, they are spin-triplet. In contrast, the other states with odd values of  $n$  are spin-singlet. The ground state with  $k = 0$  is a spin triplet, and the lowest excitations are a pair of singlets with a gap of  $t$ .

*Trimerized triangular lattice.*—Next consider the case of  $0 < |t'|/t \ll 1$ . Since the trimer ground state is spin-1,  $H'$  generates inter-trimer superexchanges and lifts the degeneracy. The weakly-coupled trimers are effectively described by the spin-1 Heisenberg model in a triangular lattice where one site represents a trimer. The effective exchange Hamiltonian reads,

$$H_{ex} = J \sum_{\langle ij \rangle} \mathbf{S}_i \cdot \mathbf{S}_j + C, \quad (3)$$

where  $\mathbf{S}_i$  represents the total spin of the trimer  $i$ ;  $J$  is the exchange energy and  $C$  is an energy constant, which will be determined below.

$J$  turns out to be FM as calculated below via the 2nd order degenerate perturbation theory. The total spin of two neighboring trimers lie in 3 channels of  $S_{\text{tot}} = 2, 1, 0$ . The energy gains in these channels are shown in SM. (IC 1), yielding that  $\Delta E^{(2)}/(\frac{t'^2}{t}) = -\frac{10}{27}, -\frac{6}{27}, -\frac{4}{27}$ , respectively. Comparing to Eq. (3), we arrive at

$$J = -\frac{2t'^2}{27t}, \quad C = 4J. \quad (4)$$

Therefore, the  $\frac{1}{3}$ -filled trimerized triangular lattice is in the FM insulating state in the limit of  $U \rightarrow \infty$  and  $t'/t \ll 1$  due to the FM exchange.

Typically the Mott insulating states give rise to the AFM superexchange due to the excitations of double occupancy. Here such excitations are suppressed by the infinite  $U$ , but the  $1/3$ -filling allows excitations free of double occupancy for the inter-trimer superexchange. To see why it is FM, we compare a FM configuration of two neighboring trimers of  $S_z = 1$  with an AFM configuration

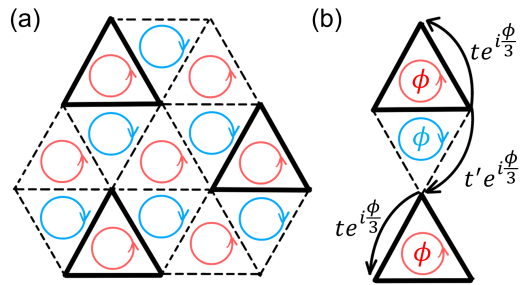


FIG. 3. (a) The trimerized triangular lattice with a staggered flux pattern  $\pm\phi$ . (b) The phase convention of hopping integrals.

exhibiting the opposite values of  $S_z = \pm 1$ . In both cases,  $H'$  generates intermediate states consisting of a 3-filled trimer and a singly filled trimer. The FM case is fully polarized, hence, all virtual hopping processes constructively interfere, while in the AFM case, the 3-filled trimer lies in different spin states, whose motion is less coherent. Hence, the kinetic energy results in the FM exchange.

*Flux threading.*—Next consider the effect of a trimerized triangular lattice with a staggered flux pattern  $\pm\phi$  threading each plaquette as shown in Fig. 3(a). Correspondingly, the intra-trimer hopping amplitude  $t$  and the inter-trimer one  $t'$  are modified as  $te^{\pm i\frac{\phi}{3}}$  and  $t'e^{\pm i\frac{\phi}{3}}$ , where the signs  $\pm$  are determined by whether the hopping is along or against the flux winding, respectively, as shown in Fig. 3(b). The flux modifies the energy spectrum of the 6 intra-trimer two-electron states as

$$E_n = -2t \cos \left( k_n + \frac{\phi}{3} \right). \quad (5)$$

Typically speaking,  $\phi$  is defined modulo  $2\pi$ . Nevertheless, the spectral flow indicated by Eq. (5) shows that the dispersion returns back at  $\phi = \pi$ , *i.e.*,  $n \rightarrow n + 1 \pmod{6}$ , but switching triplet and singlet states.

The FM exchange described in Eq. (3) remains robust at small values of  $|\phi| < \frac{\pi}{2}$  since the intra-trimer ground state remains the triplet  $|k_0\rangle$ . Nevertheless,  $J$  is reduced: The 2nd order perturbation theory shown in SM. (IC 2) shows that at  $|\phi| < \frac{\pi}{2}$  the flux dependence of  $J(\phi)$  reads

$$J(\phi) \approx J \left( 1 - \frac{7}{54} \phi^2 \right). \quad (6)$$

A more accurate expression is obtained as  $J(\phi) = -\frac{t'^2}{18t} \left( \cos \frac{2\phi}{3} \cos \frac{\phi}{3} \right) / \left( \cos \left( \frac{\phi}{3} + \frac{\pi}{6} \right) \cos \left( \frac{\phi}{3} - \frac{\pi}{6} \right) \right)$ .

When  $\phi$  reaches  $\pm\frac{\pi}{2}$ , the intra-trimer singlet and triplet states become degenerate. According to the decomposition rule of the  $SU(2)$  representations, two trimers result in 6 spin channels:  $(0 \oplus 1) \otimes (0 \oplus 1) = 0 \oplus 1 \oplus 1 \oplus 0 \oplus 1 \oplus 2$ , *i.e.*, one set of quintet ( $S_{\text{tot}} = 2$ ),

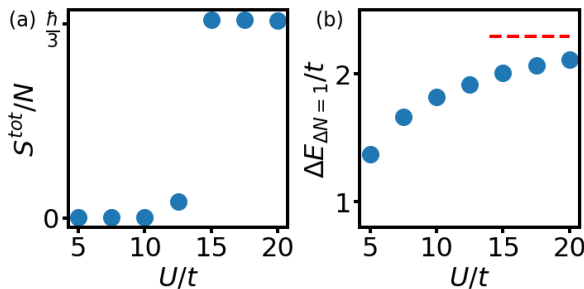


FIG. 4. The DMRG calculation for the transition to a ferromagnetic state versus  $U/t$  at  $t'/t = 0.2$ . The system is a tilted cylinder with size 4 (perimeter)  $\times$  6 (length)  $\times$  3 (unit cell size) and at  $1/3$ -filling. (a) The average spin per site  $S_{tot}/N$  reaches  $\hbar/3$  at  $U/t \gtrsim 15$ , indicating the full spin polarization. (b) The single-particle gap defined as  $\Delta E_{\Delta N=1} = E_{N=49} + E_{N=47} - 2E_{N=48}$ . The red dashed line is the band gap  $\Delta_b$  of free fermions.

three sets of triplet ( $S_{tot} = 1$ ), and two sets of singlet ( $S_{tot} = 0$ ). The perturbative energies in different sectors are calculated at the 2nd order in SM. (IC 3). The lowest and highest energy states are both spin singlets: The former is the direct-product state of two trimer singlets, and the latter is the entangled one built up by two trimer triplets, exhibiting the energies of  $\Delta E_{s,1}^{(2)} = -\frac{83t'^2}{108\sqrt{3}t}$  and  $\Delta E_{s,2}^{(2)} = -\frac{5t'^2}{12\sqrt{3}t}$ , respectively. They do not mix at the level of the 2nd order perturbation theory, nevertheless, a small mixing could occur at a high order. This means that as increasing  $|\phi|$  from 0 to  $\frac{\pi}{2}$  the ground state of the entire lattice changes from the spin fully polarized state to the direct product state of the singlet of each trimer. The transition between two different types of ground states will be deferred to a future research.

*Phase transitions by tuning  $t'$  and  $U$ .*—We now consider finite values of  $U$ , which generates the competition between AFM and FM exchanges. For simplicity only the case of  $\phi = 0$  is considered here. The intra-trimer ground states are a set of spin-1 triplet as long as  $U > 0$  as shown in SM. (IB 2), which in contrast to the case of a square that the ground state becomes spin- $\frac{3}{2}$  at a large value of  $U/t \geq 18.7$  [46]. The AFM exchange between two neighboring trimers is estimated as follows: The inter-trimer coupling is from a tip of one trimer to a bond of another trimer. When projected to the total spin of each trimer, a correction factor of  $\frac{1}{3} \times \frac{2}{3}$  is generated to the AFM exchange  $4t'^2/U$  between two singly occupied sites, yielding  $J_{AF} \approx c(t')^2/U$  with  $c$  close to 1. Then the crossing from the AFM exchange to the FM one is estimated to take place roughly at  $\frac{t'^2}{U} \sim \frac{2t'^2}{27t}$ , *i.e.*, at the order of  $U/t \sim 13$ .

The above intuitive physical picture is further refined below.  $J$  at finite values of  $U$  is calculated via the 2nd

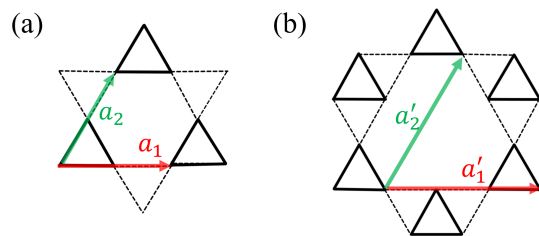


FIG. 5. (a) The trimerized Kagome lattice in which trimers form a triangular lattice. (b) The Kagome trimer lattice. Two neighboring trimers are connected via one bond in (a) and two bonds in (b), respectively.

order perturbation theory in SM. (ID 1), yielding

$$J = -\frac{2}{27} \frac{t'^2}{t} + \frac{62}{81} \frac{t'^2}{U}. \quad (7)$$

where  $1 \ll U/t < \infty$  is assumed. The transition from the AFM super-exchange to the FM one approximately takes place at  $U/t \approx 10.3$  where  $J = 0$ . Around  $J = 0$ , high-order super-exchanges should be important which will be deferred to a future research. The effects of one kind of high-order term in spin models, bilinear-biquadratic interaction, have been investigated before[47–50]. The effect of finite values of  $t'$  is studied via exact diagonalization on two neighboring trimers. The ground state switches from an SU(2) singlet to quintet as increasing  $U/t$  as shown in SM. (ID 1). The transition takes place around  $U/t \approx 13.35$  which is nearly independent on  $t'$  at  $t'/t \ll 1$ , while it starts to increase as  $t'/t > 0.2$  manifesting the growing role of higher order exchange processes, as shown in Fig. (S2).

Now consider the ground state properties of a large system. The magnetization of a 72-site system is calculated via the DMRG simulation at the  $\frac{1}{3}$ -filling with finite values of  $U$  as plotted in Fig. 4(a). At  $t'/t = 0.2$ , the transition to the fully polarized FM state occurs at  $U/t \approx 13 \sim 15$ . The partial polarization at  $U/t = 12.5$  may be due to the OBC, which will be left for further investigation. The calculated single-particle excitation gaps are plotted in Fig. 4(b), which is defined as  $\Delta E_1 = E_{N+1} + E_{N-1} - 2E_N$ , where  $E_N$  stands for the ground state energy with  $N$  particles. Upon the fully polarized state at  $U \gtrsim 15$ ,  $\Delta E_1$  is smaller than the band gap  $\Delta_b$  at finite values of  $U$  and approaches  $\Delta_b$  as  $U \rightarrow +\infty$ . Removing one fermion still maintains the system fully polarized, but an extra particle added may be anti-parallel to the background polarization forming a spin polaron to lower the energy, and this energy gain is reduced to zero at  $U/t \rightarrow +\infty$ . For the plotted paramagnetic region  $5 < U/t < 12.5$ ,  $\Delta E_1$  is smaller but comparable to the FM region.

The above studies can be easily generalized to other trimerized lattices. Fig. 5(a) shows the trimerized Kagome lattice (breathing Kagome lattice) at the  $\frac{1}{3}$ -

filling, in which two neighboring trimers only connect via one inter-trimer hopping. In the case of  $t > 0$ , the lowest band is flat with a quadratic touching with the 2nd one. The widths of the 2nd and 3rd bands are at the order of  $|t'|$ , and these bands are separated by the gap  $\Delta_b \sim t$ . When the flat-band is half-filled, *i.e.*, the  $\frac{1}{6}$ -filling, the system is FM which should be stable with respect to small dopings away from the  $\frac{1}{6}$ -filling. Nevertheless, as shown in SM. (ID 2), the exchange between two neighboring trimers at the  $\frac{1}{3}$ -filling in the regime  $U \gg t \gg t'$  turns out to be AFM. In fact, the exchange disappears at  $U/t = \infty$  because no spin-flip process takes place via a single link connecting two trimers. Finite  $U$  renders spin-flip processes feasible yielding the same Hamiltonian as Eq. (4) with the AFM exchange  $J = \frac{44}{81} \frac{t'^2}{U}$  and  $C = -\left(\frac{4}{27} \frac{t'^2}{t} + \frac{44}{81} \frac{t'^2}{U}\right)$ . Since the trimers form a triangular lattice, the system will exhibit the  $120^\circ$  pattern of the AMF order. The lattice shown in Fig. 5 (b) is dubbed the Kagome trimer lattice, where trimers form a Kagome lattice and the connection between neighbouring trimers is via two bonds, hence, the superexchange will be the same as in Eq. (7). Therefore, as increasing  $U/t$ , the effective model will also undergo a transition from the spin-1 AFM Heisenberg model to the FM one in the Kagome lattice.

It would be interesting to further explore the physics by doping the  $1/3$ -filling correlated insulating state in the triangular lattice. When the FM superexchange dominates, the system will become a FM metal upon slight hole dopplings. The doped holes move in the background of FM-coupled spin-1 moments, which are still polarized. On the other hand, if the AFM superexchange dominates, the interplay between hole mobility and magnetic frustrations would generate rich physics for further explorations.

*Conclusion.*—We have shown that a FM insulating state is established in the trimerized triangular lattice at the  $\frac{1}{3}$ -filling with  $t > 0$  in the regime of  $U \gg t \gg |t'|$ . In each trimer, two electrons form spin-1 moments due to the “orbital” degeneracy and repulsive interaction. The inter-trimer hoppings generate superexchange couplings to lower the kinetic energy. At  $U/t \rightarrow \infty$ , only the FM superexchange exists, which is weakened by introducing a staggered flux pattern in the lattice. As  $U/t$  becomes finite, both the FM and AFM superexchanges contribute, and the former wins over the latter around  $U/t \gtrsim 15$ . This work provides valuable insights into the study of quantum magnetism in correlated fermion systems.

We are grateful for the stimulating discussions with Zhiming Pan. CW is supported by the National Natural Science Foundation of China under the Grant No. 12234016 and No. 12174317. YH is supported by European Research Council (ERC) under the European Union Horizon 2020 Research and Innovation

Programme (Grant Agreement Nos. 804213-TMCS). The QuSpin [51] and TeNPy [45] packages were used for the numerical studies. This work has been supported by the New Cornerstone Science Foundation.

---

\* yuchi.he@physics.ox.ac.uk

† wucongjun@westlake.edu.cn

- [1] J. Kanamori, Electron Correlation and Ferromagnetism of Transition Metals, Progress of Theoretical Physics **30**, 275 (1963).
- [2] Y. Nagaoka, Ferromagnetism in a Narrow, Almost Half-Filled  $s$  Band, Phys. Rev. **147**, 392 (1966).
- [3] J. O. Haerter and B. S. Shastry, Kinetic Antiferromagnetism in the Triangular Lattice, Phys. Rev. Lett. **95**, 087202 (2005).
- [4] A. Mielke, Exact ground states for the Hubbard model on the Kagome lattice, Journal of Physics A: Mathematical and General **25**, 4335 (1992).
- [5] A. Mielke, Ferromagnetism in the Hubbard model and Hund’s rule, Physics Letters A **174**, 443 (1993).
- [6] A. Mielke and H. Tasaki, Ferromagnetism in the Hubbard model, Communications in Mathematical Physics **158**, 341 (1993).
- [7] H. Tasaki, Ferromagnetism in Hubbard Models, Phys. Rev. Lett. **75**, 4678 (1995).
- [8] H. Tasaki, Stability of ferromagnetism in Hubbard models with nearly flat bands, Journal of Statistical Physics **84**, 535 (1996).
- [9] Y. Li, E. H. Lieb, and C. Wu, Exact Results for Itinerant Ferromagnetism in Multiorbital Systems on Square and Cubic Lattices, Phys. Rev. Lett. **112**, 217201 (2014).
- [10] S. Xu, Y. Li, and C. Wu, Sign-Problem-Free Quantum Monte Carlo Study on Thermodynamic Properties and Magnetic Phase Transitions in Orbital-Active Itinerant Ferromagnets, Phys. Rev. X **5**, 021032 (2015).
- [11] N. F. Mott, The Basis of the Electron Theory of Metals, with Special Reference to the Transition Metals, Proceedings of the Physical Society. Section A **62**, 416 (1949).
- [12] P. Anderson, Resonating valence bonds: A new kind of insulator?, Materials Research Bulletin **8**, 153 (1973).
- [13] P. A. Lee, N. Nagaosa, and X.-G. Wen, Doping a Mott insulator: Physics of high-temperature superconductivity, Rev. Mod. Phys. **78**, 17 (2006).
- [14] M. R. Norman, Colloquium: Herbertsmithite and the search for the quantum spin liquid, Rev. Mod. Phys. **88**, 041002 (2016).
- [15] K. Kanoda and R. Kato, Mott Physics in Organic Conductors with Triangular Lattices, Annual Review of Condensed Matter Physics **2**, 167 (2011).
- [16] S. Sachdev, Quantum phases and phase transitions of Mott insulators, in *Quantum Magnetism*, edited by U. Schollwöck, J. Richter, D. J. J. Farnell, and R. F. Bishop (Springer Berlin Heidelberg, Berlin, Heidelberg, 2004) pp. 381–432.
- [17] A. Vasiliev, O. Volkova, E. Zvereva, and M. Markina, Milestones of low-D quantum magnetism, npj Quantum Materials **3**, 18 (2018).
- [18] L. Savary and L. Balents, Quantum spin liquids: a review, Reports on Progress in Physics **80**, 016502

- (2016).
- [19] D. I. Khomskii and S. V. Streltsov, Orbital Effects in Solids: Basics, Recent Progress, and Opportunities, *Chemical Reviews* **121**, 2992 (2021), publisher: American Chemical Society.
- [20] H. Yao and S. A. Kivelson, Fragile Mott Insulators, *Phys. Rev. Lett.* **105**, 166402 (2010).
- [21] W.-Y. He, X. Y. Xu, G. Chen, K. T. Law, and P. A. Lee, Spinon Fermi Surface in a Cluster Mott Insulator Model on a Triangular Lattice and Possible Application to  $1T$ -TaS<sub>2</sub>, *Phys. Rev. Lett.* **121**, 046401 (2018).
- [22] J. Hu, X. Zhang, C. Hu, J. Sun, X. Wang, H.-Q. Lin, and G. Li, Correlated flat bands and quantum spin liquid state in a cluster Mott insulator, *Communications Physics* **6**, 172 (2023).
- [23] F. Foggetti, S.-W. Cheong, and S. Artyukhin, Magnetic monopoles and toroidal moments in  $\text{LuFeO}_3$  and related compounds, *Phys. Rev. B* **100**, 180408 (2019).
- [24] S. A. Nikolaev, I. V. Solov'yev, and S. V. Streltsov, Quantum spin liquid and cluster Mott insulator phases in the  $\text{Mo}_3\text{O}_8$  magnets, *npj Quantum Materials* **6**, 25 (2021).
- [25] A. Akbari-Sharbat, R. Sinclair, A. Verrier, D. Ziat, H. D. Zhou, X. F. Sun, and J. A. Quilliam, Tunable Quantum Spin Liquidity in the  $1/6$ th-Filled Breathing Kagome Lattice, *Phys. Rev. Lett.* **120**, 227201 (2018).
- [26] G. Chen and P. A. Lee, Emergent orbitals in the cluster Mott insulator on a breathing Kagome lattice, *Phys. Rev. B* **97**, 035124 (2018).
- [27] P. Gall, R. A. R. A. Orabi, T. Guizouarn, and P. Gougeon, Synthesis, crystal structure and magnetic properties of  $\text{Li}_2\text{InMo}_3\text{O}_8$ : A novel reduced molybdenum oxide containing magnetic  $\text{Mo}_3$  clusters, *Journal of Solid State Chemistry* **208**, 99 (2013).
- [28] C. C. Torardi and R. E. McCarley, Synthesis, crystal structures, and properties of lithium zinc molybdenum oxide ( $\text{LiZn}_2\text{Mo}_3\text{O}_8$ ), zinc molybdenum oxide ( $\text{Zn}_3\text{Mo}_3\text{O}_8$ ), and scandium zinc molybdenum oxide ( $\text{ScZnMo}_3\text{O}_8$ ), reduced derivatives containing the  $\text{Mo}_3\text{O}_{13}$  cluster unit, *Inorganic Chemistry* **24**, 476 (1985), publisher: American Chemical Society.
- [29] M. Okumura, S. Yamada, M. Machida, and H. Aoki, Phase-separated ferromagnetism in a spin-imbalanced system of Fermi atoms loaded in an optical ladder: A density-matrix renormalization-group study, *Phys. Rev. A* **83**, 031606 (2011).
- [30] I. Morera, M. Kanász-Nagy, T. Smolenski, L. Ciorciaro, A. m. c. Imamoğlu, and E. Demler, High-temperature kinetic magnetism in triangular lattices, *Phys. Rev. Res.* **5**, L022048 (2023).
- [31] C. Li, M.-G. He, C.-Y. Wang, and H. Zhai, Frustration-induced itinerant ferromagnetism of fermions in optical lattices, *Phys. Rev. B* **109**, 165131 (2024).
- [32] R. Samajdar and R. N. Bhatt, Nagaoka ferromagnetism in doped Hubbard models in optical lattices, *Phys. Rev. A* **110**, L021303 (2024).
- [33] R. Samajdar and R. N. Bhatt, Polaronic mechanism of Nagaoka ferromagnetism in Hubbard models, *Phys. Rev. B* **109**, 235128 (2024).
- [34] J. von Stecher, E. Demler, M. D. Lukin, and A. M. Rey, Probing interaction-induced ferromagnetism in optical superlattices, *New Journal of Physics* **12**, 055009 (2010).
- [35] M. Lebrat, M. Xu, L. H. Kendrick, A. Kale, Y. Gang, P. Seetharaman, I. Morera, E. Khatami, E. Demler, and M. Greiner, Observation of Nagaoka polarons in a Fermi-Hubbard quantum simulator, *Nature* **629**, 317 (2024).
- [36] G. V. Chen and C. Wu, Multiflavor Mott insulators in quantum materials and ultracold atoms, *npj Quantum Materials* **9**, 1 (2024).
- [37] T. Hanisch, B. Kleine, A. Ritzl, and E. M. Eller-Hartmann, Ferromagnetism in the Hubbard model: instability of the Nagaoka state on the triangular, honeycomb and kagome lattices, *Annalen der Physik* **507**, 303 (1995).
- [38] M. Xu, L. H. Kendrick, A. Kale, Y. Gang, G. Ji, R. T. Scalettar, M. Lebrat, and M. Greiner, Frustration- and doping-induced magnetism in a Fermi-Hubbard simulator, *Nature* **620**, 971 (2023).
- [39] G. Li, A. E. Antipov, A. N. Rubtsov, S. Kirchner, and W. Hanke, Competing phases of the Hubbard model on a triangular lattice: Insights from the entropy, *Phys. Rev. B* **89**, 161118 (2014).
- [40] K. Lee, P. Sharma, O. Vafek, and H. J. Changlani, Triangular lattice Hubbard model physics at intermediate temperatures, *Phys. Rev. B* **107**, 235105 (2023).
- [41] Y. He, R. Rausch, M. Peschke, C. Karrasch, P. Corboz, N. Bultinck, and S. A. Parameswaran, Itinerant Magnetism in the Triangular Lattice Hubbard Model at Half-doping: Application to Twisted Transition-Metal Dichalcogenides (2023), arXiv:2311.10146 [cond-mat.str-el].
- [42] I. Morera and E. Demler, Itinerant magnetism and magnetic polarons in the triangular lattice Hubbard model (2024), arXiv:2402.14074 [cond-mat.str-el].
- [43] Q. Chen, S. A. Chen, and Z. Zhu, Ferromagnetism Mechanism in a Geometrically Frustrated Triangular Lattice (2024), arXiv:2408.05971 [cond-mat.str-el].
- [44] S. R. White, Density matrix formulation for quantum renormalization groups, *Phys. Rev. Lett.* **69**, 2863 (1992).
- [45] J. Hauschild and F. Pollmann, Efficient numerical simulations with Tensor Networks: Tensor Network Python (TeNPy), *SciPost Phys. Lect. Notes* , 5 (2018), code available from <https://github.com/tenpy/tenpy>, arXiv:1805.00055.
- [46] J. P. Dehollain, U. Mukhopadhyay, V. P. Michal, Y. Wang, B. Wunsch, C. Reichl, W. Wegscheider, M. S. Rudner, E. Demler, and L. M. K. Vandersypen, Nagaoka ferromagnetism observed in a quantum dot plaquette, *Nature* **579**, 528 (2020).
- [47] H. Tsunetsugu and M. Arikawa, Spin Nematic Phase in  $S=1$  Triangular Antiferromagnets, *Journal of the Physical Society of Japan* **75**, 083701 (2006), <https://doi.org/10.1143/JPSJ.75.083701>.
- [48] P. Corboz, A. M. Läuchli, K. Penc, M. Troyer, and F. Mila, Simultaneous Dimerization and  $SU(4)$  Symmetry Breaking of 4-Color Fermions on the Square Lattice, *Phys. Rev. Lett.* **107**, 215301 (2011), publisher: American Physical Society.
- [49] S. Bhattacharjee, V. B. Shenoy, and T. Senthil, Possible ferro-spin nematic order in  $\text{NiGa}_2\text{S}_4$ , *Phys. Rev. B* **74**, 092406 (2006).
- [50] E. M. Stoudenmire, S. Trebst, and L. Balents, Quadrupolar correlations and spin freezing in  $S = 1$  triangular lattice antiferromagnets, *Phys. Rev. B* **79**, 214436 (2009).
- [51] P. Weinberg and M. Bukov, QuSpin: a Python Package for Dynamics and Exact Diagonalisation of Quantum

Many Body Systems. Part II: bosons, fermions and higher spins, SciPost Phys. **7**, 20 (2019).

## I. SUPPLEMENTAL MATERIAL

### A. The spectrum of $t - t'$ triangular lattice

The calculation detail of free band structure is shown below. Considering the free form of Hamiltonian (1) in momentum space, we obtain the Bloch form in the Bloch basis as

$$\begin{pmatrix} 0 & t + t' \left( e^{-i\vec{k}\cdot\vec{a}_1} + e^{-i\vec{k}\cdot\vec{a}_2} \right) & t + t' e^{-i\vec{k}\cdot\vec{a}_1} \left( 1 + e^{i\vec{k}\cdot\vec{a}_2} \right) \\ t + t' \left( e^{i\vec{k}\cdot\vec{a}_1} + e^{i\vec{k}\cdot\vec{a}_2} \right) & 0 & t + t' e^{i\vec{k}\cdot\vec{a}_1} \left( 1 + e^{-i\vec{k}\cdot\vec{a}_2} \right) \\ t + t' e^{i\vec{k}\cdot\vec{a}_1} \left( 1 + e^{-i\vec{k}\cdot\vec{a}_2} \right) & t + t' e^{-i\vec{k}\cdot\vec{a}_1} \left( 1 + e^{i\vec{k}\cdot\vec{a}_2} \right) & 0 \end{pmatrix} \quad (\text{S1})$$

where  $\vec{k} = (k_x, k_y)$  and  $\vec{a}_1 = (0, \sqrt{3})$ ,  $\vec{a}_2 = (\frac{3}{2}, \frac{\sqrt{3}}{2})$ . For disconnected trimers ( $t' = 0$ ), the matrix is reduced to the form

$$\begin{pmatrix} 0 & t & t \\ t & 0 & t \\ t & t & 0 \end{pmatrix} \quad (\text{S2})$$

and the spectrum consists of three flat bands:  $\varepsilon_1 = \varepsilon_2 = -t$ ,  $\varepsilon_3 = 2t$ . For connected ones, the eigen-value satisfies a cubic equation

$$\varepsilon^3 - p\varepsilon + q = 0$$

where

$$p = \left| t + t' \left( e^{-i\vec{k}\cdot\vec{a}_1} + e^{-i\vec{k}\cdot\vec{a}_2} \right) \right|^2 + 2 \left| t + t' e^{-i\vec{k}\cdot\vec{a}_1} \left( 1 + e^{i\vec{k}\cdot\vec{a}_2} \right) \right|^2$$

$$q = -2 \left| t + t' e^{-i\vec{k}\cdot\vec{a}_1} \left( 1 + e^{i\vec{k}\cdot\vec{a}_2} \right) \right|^2 \text{Re} \left( t + t' \left( e^{-i\vec{k}\cdot\vec{a}_1} + e^{-i\vec{k}\cdot\vec{a}_2} \right) \right)$$

Then with cubic formula

$$\varepsilon_1 = \left( \frac{q}{2} + \sqrt{\frac{q^2}{4} - \frac{p^3}{27}} \right)^{\frac{1}{3}} + \left( -\frac{q}{2} + \sqrt{\frac{q^2}{4} - \frac{p^3}{27}} \right)^{\frac{1}{3}}$$

$$\varepsilon_2 = e^{i\frac{2\pi}{3}} \left( \frac{q}{2} + \sqrt{\frac{q^2}{4} - \frac{p^3}{27}} \right)^{\frac{1}{3}} + e^{-i\frac{2\pi}{3}} \left( -\frac{q}{2} + \sqrt{\frac{q^2}{4} - \frac{p^3}{27}} \right)^{\frac{1}{3}}$$

$$\varepsilon_3 = e^{-i\frac{2\pi}{3}} \left( \frac{q}{2} + \sqrt{\frac{q^2}{4} - \frac{p^3}{27}} \right)^{\frac{1}{3}} + e^{i\frac{2\pi}{3}} \left( -\frac{q}{2} + \sqrt{\frac{q^2}{4} - \frac{p^3}{27}} \right)^{\frac{1}{3}}$$

the free band structure is solved, as depicted in Fig. S1 in terms of  $t'/t$ . We see that the band width is proportional to  $t'$ , and is closing during the increase in inter-trimers hopping.

### B. Single trimer at finite $U$

We solve the Hamiltonian  $H_0$  of a single trimer below half-filling, which is the starting point of degenerate perturbation theory.

#### 1. $n = 1$

With only 1 electron, it's reduced to a single-particle problem. Due to the SU(2) symmetry, it's enough to consider  $S_z = \frac{1}{2}$  sector only. Trimer has  $C_3$  symmetry, and this symmetry encourages us to classify all the  $S_z = \frac{1}{2}$  states as  $|k = -\frac{2\pi}{3}\rangle = \frac{e^{-2\pi/3}c_{1\uparrow}^\dagger + e^{2\pi/3}c_{2\uparrow}^\dagger + c_{3\uparrow}^\dagger}{3}|\Omega\rangle$ ,  $|k = \frac{2\pi}{3}\rangle = \frac{e^{2\pi/3}c_{1\uparrow}^\dagger + e^{-2\pi/3}c_{2\uparrow}^\dagger + c_{3\uparrow}^\dagger}{3}|\Omega\rangle$ ,  $|k = 0\rangle = \frac{c_{1\uparrow}^\dagger + c_{2\uparrow}^\dagger + c_{3\uparrow}^\dagger}{3}|\Omega\rangle$  which is exactly

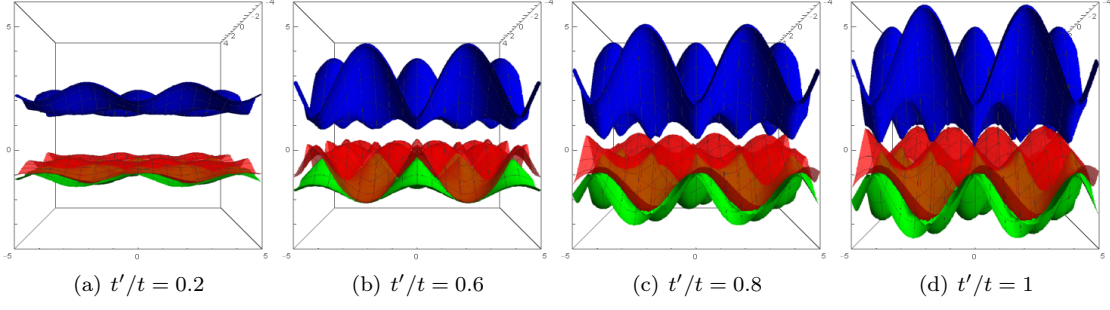


FIG. S1. The band structure of fully polarized sector from  $t'/t = 0$  to  $t'/t = 1$ .

the eigen-states because they're labeled with different good quantum number. The corresponding eigen-energies are  $-t, -t, 2t$ .

The solution with flux is similar. The eigen-states are the same since  $C_3$  symmetry is preserved after inserting flux, and the eigen-energies are now adjusted as  $2t \cos(\theta - \frac{2}{3}\pi), 2t \cos(\theta + \frac{2}{3}\pi), 2t \cos \theta$ , where we define  $\phi/3 = \theta$  for simplicity. This convention is kept below.

## 2. $n = 2$

In the main text, the solution is introduced at  $U = \infty$ . Below the result is extended in the regime of finite  $U$ .

Due to  $SU(2)$  symmetry, considering  $S_z = 0$  sector only, there's 9 configurations in Hilbert space, and according to  $C_3$  symmetry, they're further classified into three sector

$$\begin{aligned}
|\varphi_1, k = 0\rangle &= \frac{1}{\sqrt{3}} \left( c_{1\uparrow}^\dagger c_{2\downarrow}^\dagger + c_{2\uparrow}^\dagger c_{3\downarrow}^\dagger + c_{3\uparrow}^\dagger c_{1\downarrow}^\dagger \right) |\Omega\rangle \\
|\varphi_2, k = 0\rangle &= \frac{1}{\sqrt{3}} \left( c_{1\downarrow}^\dagger c_{2\uparrow}^\dagger + c_{2\downarrow}^\dagger c_{3\uparrow}^\dagger + c_{3\downarrow}^\dagger c_{1\uparrow}^\dagger \right) |\Omega\rangle \\
|\varphi_3, k = 0\rangle &= \frac{1}{\sqrt{3}} \left( c_{1\uparrow}^\dagger c_{1\downarrow}^\dagger + c_{2\uparrow}^\dagger c_{2\downarrow}^\dagger + c_{3\uparrow}^\dagger c_{3\downarrow}^\dagger \right) |\Omega\rangle \\
|\varphi_1, k = \frac{2\pi}{3}\rangle &= \frac{1}{\sqrt{3}} \left( c_{1\uparrow}^\dagger c_{2\downarrow}^\dagger + e^{i\frac{2\pi}{3}} c_{2\uparrow}^\dagger c_{3\downarrow}^\dagger + e^{-i\frac{2\pi}{3}} c_{3\uparrow}^\dagger c_{1\downarrow}^\dagger \right) |\Omega\rangle \\
|\varphi_2, k = \frac{2\pi}{3}\rangle &= \frac{1}{\sqrt{3}} \left( c_{1\downarrow}^\dagger c_{2\uparrow}^\dagger + e^{i\frac{2\pi}{3}} c_{2\downarrow}^\dagger c_{3\uparrow}^\dagger + e^{-i\frac{2\pi}{3}} c_{3\downarrow}^\dagger c_{1\uparrow}^\dagger \right) |\Omega\rangle \\
|\varphi_3, k = \frac{2\pi}{3}\rangle &= \frac{1}{\sqrt{3}} \left( c_{1\uparrow}^\dagger c_{1\downarrow}^\dagger + e^{i\frac{2\pi}{3}} c_{2\uparrow}^\dagger c_{2\downarrow}^\dagger + e^{-i\frac{2\pi}{3}} c_{3\uparrow}^\dagger c_{3\downarrow}^\dagger \right) |\Omega\rangle \\
|\varphi_1, k = -\frac{2\pi}{3}\rangle &= \frac{1}{\sqrt{3}} \left( c_{1\uparrow}^\dagger c_{2\downarrow}^\dagger + e^{-i\frac{2\pi}{3}} c_{2\uparrow}^\dagger c_{3\downarrow}^\dagger + e^{i\frac{2\pi}{3}} c_{3\uparrow}^\dagger c_{1\downarrow}^\dagger \right) |\Omega\rangle \\
|\varphi_2, k = -\frac{2\pi}{3}\rangle &= \frac{1}{\sqrt{3}} \left( c_{1\downarrow}^\dagger c_{2\uparrow}^\dagger + e^{-i\frac{2\pi}{3}} c_{2\downarrow}^\dagger c_{3\uparrow}^\dagger + e^{i\frac{2\pi}{3}} c_{3\downarrow}^\dagger c_{1\uparrow}^\dagger \right) |\Omega\rangle \\
|\varphi_3, k = -\frac{2\pi}{3}\rangle &= \frac{1}{\sqrt{3}} \left( c_{1\uparrow}^\dagger c_{1\downarrow}^\dagger + e^{-i\frac{2\pi}{3}} c_{2\uparrow}^\dagger c_{2\downarrow}^\dagger + e^{i\frac{2\pi}{3}} c_{3\uparrow}^\dagger c_{3\downarrow}^\dagger \right) |\Omega\rangle
\end{aligned}$$

which is labeled by different good quantum number  $k$ . For each  $k = 0, \frac{2\pi}{3}, -\frac{2\pi}{3}$  sector, the Hamiltonian is reduced into three  $3 \times 3$  matrices listed below

$$\begin{pmatrix} 0 & -2t & 2t \\ -2t & 0 & -2t \\ 2t & -2t & U \end{pmatrix}, \begin{pmatrix} 0 & -t & te^{i\frac{\pi}{3}} \\ -t & 0 & te^{-i\frac{\pi}{3}} \\ te^{-i\frac{\pi}{3}} & te^{i\frac{\pi}{3}} & U \end{pmatrix}, \begin{pmatrix} 0 & -t & te^{-i\frac{\pi}{3}} \\ -t & 0 & te^{i\frac{\pi}{3}} \\ te^{i\frac{\pi}{3}} & te^{-i\frac{\pi}{3}} & U \end{pmatrix} \quad (S3)$$

Noting that as long as  $U > 0$ , the GS is triplet.

When  $U \gg t$ , the results goes back to Eq. (2) for 6 states without double occupation, and for other 3 double occupation states, the energy is  $U$ . For convenience of following discussion, we write down GS here and denote them

as:

$$\begin{aligned}
|1, 0\rangle &= \frac{1}{\sqrt{6}} \left( c_{1\uparrow}^\dagger c_{2\downarrow}^\dagger + c_{1\downarrow}^\dagger c_{2\uparrow}^\dagger + c_{2\uparrow}^\dagger c_{3\downarrow}^\dagger + c_{2\downarrow}^\dagger c_{3\uparrow}^\dagger + c_{3\uparrow}^\dagger c_{1\downarrow}^\dagger + c_{3\downarrow}^\dagger c_{1\uparrow}^\dagger \right) |\Omega\rangle \\
|1, 1\rangle &= S_+ |1, 0\rangle = \frac{1}{\sqrt{3}} \left( c_{1\uparrow}^\dagger c_{2\uparrow}^\dagger + c_{2\uparrow}^\dagger c_{3\uparrow}^\dagger + c_{3\uparrow}^\dagger c_{1\uparrow}^\dagger \right) |\Omega\rangle \\
|1, -1\rangle &= S_- |1, 0\rangle = |1, -1\rangle = \frac{1}{\sqrt{3}} \left( c_{1\downarrow}^\dagger c_{2\downarrow}^\dagger + c_{2\downarrow}^\dagger c_{3\downarrow}^\dagger + c_{3\downarrow}^\dagger c_{1\downarrow}^\dagger \right) |\Omega\rangle
\end{aligned} \tag{S4}$$

### 3. $n = 3$

Due to SU(2) symmetry, here consider the states for  $S_z = \frac{1}{2}$  sector only, which can be further classified into three sectors according to good quantum number  $k$ :

$$\begin{aligned}
|\psi_1, k = 0\rangle &= \frac{1}{\sqrt{3}} \left( c_{1\uparrow}^\dagger c_{2\uparrow}^\dagger c_{3\downarrow}^\dagger + c_{1\uparrow}^\dagger c_{2\downarrow}^\dagger c_{3\uparrow}^\dagger + c_{1\downarrow}^\dagger c_{2\uparrow}^\dagger c_{3\uparrow}^\dagger \right) |\Omega\rangle \\
|\psi_2, k = 0\rangle &= \frac{1}{\sqrt{3}} \left( c_{1\uparrow}^\dagger c_{1\downarrow}^\dagger c_{2\uparrow}^\dagger + c_{2\uparrow}^\dagger c_{2\downarrow}^\dagger c_{3\uparrow}^\dagger + c_{3\uparrow}^\dagger c_{3\downarrow}^\dagger c_{1\uparrow}^\dagger \right) |\Omega\rangle \\
|\psi_3, k = 0\rangle &= \frac{1}{\sqrt{3}} \left( c_{1\uparrow}^\dagger c_{1\downarrow}^\dagger c_{3\uparrow}^\dagger + c_{2\uparrow}^\dagger c_{2\downarrow}^\dagger c_{1\uparrow}^\dagger + c_{3\uparrow}^\dagger c_{3\downarrow}^\dagger c_{2\uparrow}^\dagger \right) |\Omega\rangle \\
|\psi_1, k = \frac{2\pi}{3}\rangle &= \frac{1}{\sqrt{3}} \left( c_{1\uparrow}^\dagger c_{2\uparrow}^\dagger c_{3\downarrow}^\dagger + e^{i\frac{2\pi}{3}} c_{1\uparrow}^\dagger c_{2\downarrow}^\dagger c_{3\uparrow}^\dagger + e^{-i\frac{2\pi}{3}} c_{1\downarrow}^\dagger c_{2\uparrow}^\dagger c_{3\uparrow}^\dagger \right) |\Omega\rangle \\
|\psi_2, k = \frac{2\pi}{3}\rangle &= \frac{1}{\sqrt{3}} \left( c_{1\uparrow}^\dagger c_{1\downarrow}^\dagger c_{2\uparrow}^\dagger + e^{i\frac{2\pi}{3}} c_{2\uparrow}^\dagger c_{2\downarrow}^\dagger c_{3\uparrow}^\dagger + e^{-i\frac{2\pi}{3}} c_{3\uparrow}^\dagger c_{3\downarrow}^\dagger c_{1\uparrow}^\dagger \right) |\Omega\rangle \\
|\psi_3, k = \frac{2\pi}{3}\rangle &= \frac{1}{\sqrt{3}} \left( c_{1\uparrow}^\dagger c_{1\downarrow}^\dagger c_{3\uparrow}^\dagger + e^{i\frac{2\pi}{3}} c_{2\uparrow}^\dagger c_{2\downarrow}^\dagger c_{1\uparrow}^\dagger + e^{-i\frac{2\pi}{3}} c_{3\uparrow}^\dagger c_{3\downarrow}^\dagger c_{2\uparrow}^\dagger \right) |\Omega\rangle \\
|\psi_1, k = -\frac{2\pi}{3}\rangle &= \frac{1}{\sqrt{3}} \left( c_{1\uparrow}^\dagger c_{2\uparrow}^\dagger c_{3\downarrow}^\dagger + e^{-i\frac{2\pi}{3}} c_{1\uparrow}^\dagger c_{2\downarrow}^\dagger c_{3\uparrow}^\dagger + e^{i\frac{2\pi}{3}} c_{1\downarrow}^\dagger c_{2\uparrow}^\dagger c_{3\uparrow}^\dagger \right) |\Omega\rangle \\
|\psi_2, k = -\frac{2\pi}{3}\rangle &= \frac{1}{\sqrt{3}} \left( c_{1\uparrow}^\dagger c_{1\downarrow}^\dagger c_{2\uparrow}^\dagger + e^{-i\frac{2\pi}{3}} c_{2\uparrow}^\dagger c_{2\downarrow}^\dagger c_{3\uparrow}^\dagger + e^{i\frac{2\pi}{3}} c_{3\uparrow}^\dagger c_{3\downarrow}^\dagger c_{1\uparrow}^\dagger \right) |\Omega\rangle \\
|\psi_3, k = -\frac{2\pi}{3}\rangle &= \frac{1}{\sqrt{3}} \left( c_{1\uparrow}^\dagger c_{1\downarrow}^\dagger c_{3\uparrow}^\dagger + e^{-i\frac{2\pi}{3}} c_{2\uparrow}^\dagger c_{2\downarrow}^\dagger c_{1\uparrow}^\dagger + e^{i\frac{2\pi}{3}} c_{3\uparrow}^\dagger c_{3\downarrow}^\dagger c_{2\uparrow}^\dagger \right) |\Omega\rangle
\end{aligned}$$

The Hamiltonian is reduced to the direct sum of three  $3 \times 3$  matrices, which is written below, separately:

$$\begin{pmatrix} 0 & & \\ U & & \\ & U & \end{pmatrix}, \begin{pmatrix} 0 & \sqrt{3}te^{-i\frac{5\pi}{6}} & \sqrt{3}te^{i\frac{\pi}{2}} \\ \sqrt{3}te^{i\frac{5\pi}{6}} & U & \sqrt{3}te^{-i\frac{\pi}{6}} \\ \sqrt{3}te^{-i\frac{\pi}{2}} & \sqrt{3}te^{i\frac{\pi}{6}} & U \end{pmatrix}, \begin{pmatrix} 0 & \sqrt{3}te^{i\frac{5\pi}{6}} & \sqrt{3}te^{-i\frac{\pi}{2}} \\ \sqrt{3}te^{-i\frac{5\pi}{6}} & U & \sqrt{3}te^{i\frac{\pi}{6}} \\ \sqrt{3}te^{i\frac{\pi}{2}} & \sqrt{3}te^{-i\frac{\pi}{6}} & U \end{pmatrix} \tag{S5}$$

Noting that the states belonging to  $k = 0$  sectors do not mix up with each other spontaneously.

When  $U \gg t$ , the eigen-states and eigen-energies are listed below

$$\begin{aligned}
|\psi_1, 0\rangle & & 0 \\
|\bar{\psi}_1, \pm \frac{2\pi}{3}\rangle &= |\psi_1, \pm \frac{2\pi}{3}\rangle - \frac{\sqrt{3}t}{U} \left( e^{\pm i\frac{5\pi}{6}} |\psi_2, \pm \frac{2\pi}{3}\rangle + e^{\mp i\frac{\pi}{2}} |\psi_3, \pm \frac{2\pi}{3}\rangle \right) & -\frac{6t^2}{U} \\
|\psi_2, 0\rangle & & U \\
|\psi_3, 0\rangle & & U \\
|\psi_{\pm}, \frac{2\pi}{3}\rangle &= \frac{1}{\sqrt{2}} \left( |\psi_2, \frac{2\pi}{3}\rangle \pm e^{i\frac{\pi}{6}} |\psi_3, \frac{2\pi}{3}\rangle \right) & U \pm \sqrt{3}t \\
|\psi_{\pm}, -\frac{2\pi}{3}\rangle &= \frac{1}{\sqrt{2}} \left( |\psi_2, -\frac{2\pi}{3}\rangle \pm e^{-i\frac{\pi}{6}} |\psi_3, -\frac{2\pi}{3}\rangle \right) & U \pm \sqrt{3}t
\end{aligned} \tag{S6}$$

Further, the energies of  $|\psi_{\pm}, \pm \frac{2\pi}{3}\rangle$  can be approximated as  $U$  with the condition  $U \gg t$ , and it allows to consider  $c_{i\uparrow}^\dagger c_{i\downarrow}^\dagger c_{j\uparrow}^\dagger |\Omega\rangle$ ,  $i \neq j$  as eigen-states directly.

In this section, we have solved all the eigen-states and eigen-energies of single trimer below and at half-filling, with the convention of positive  $t$ . For the one above half-filling problem, with particle-hole transformation, the result can be obtained by simply  $t \rightarrow -t$ .

### C. The 2nd order degenerate perturbation theory

#### 1. Without flux

The calculation process of 2nd energy correction is tedious, thus we put some key calculation steps here for reference.

We have solved the eigen-state of a single trimer with 2 electrons for  $S_z = 0$  sector, the ground-state(GS) of which is  $|k_0\rangle$ . The perturbation  $t'$  opens three channels between two trimers, which are  $|S = 2\rangle = |1, 1\rangle_A |1, 1\rangle_B$ ,  $|S = 1\rangle = \frac{1}{\sqrt{2}} (|1, 1\rangle_A |1, 0\rangle_B - |1, 0\rangle_A |1, 1\rangle_B)$ ,  $|S = 0\rangle = \frac{1}{\sqrt{3}} (|1, 1\rangle_A |1, -1\rangle_B - |1, 0\rangle_A |1, 0\rangle_B + |1, -1\rangle_A |1, 1\rangle_B)$ . With the calculation of intermediate states

$$\begin{aligned}
H'|S = 2\rangle &= -\frac{t'}{3} \left( \sqrt{2} c_{1'\uparrow}^\dagger c_{2'\uparrow}^\dagger c_{3'\uparrow}^\dagger \frac{c_{2\uparrow}^\dagger - c_{1\uparrow}^\dagger}{\sqrt{2}} + 2\sqrt{2} c_{1'\uparrow}^\dagger c_{2'\uparrow}^\dagger c_{3'\uparrow}^\dagger \frac{c_{2'\uparrow}^\dagger - c_{1'\uparrow}^\dagger}{\sqrt{2}} \right) |\Omega\rangle \\
H'|S = 1\rangle &= -\frac{t'}{6} \left( -2\sqrt{2} c_{1'\uparrow}^\dagger c_{2'\uparrow}^\dagger c_{3'\downarrow}^\dagger \frac{c_{1'\uparrow}^\dagger - c_{2'\uparrow}^\dagger}{\sqrt{2}} \right. \\
&\quad + 2\sqrt{2} c_{1'\uparrow}^\dagger c_{2'\uparrow}^\dagger c_{3'\uparrow}^\dagger \frac{c_{1'\downarrow}^\dagger - c_{2'\downarrow}^\dagger}{\sqrt{2}} - \sqrt{2} \frac{c_{1\downarrow}^\dagger - c_{2\downarrow}^\dagger}{\sqrt{2}} c_{1'\uparrow}^\dagger c_{2'\uparrow}^\dagger c_{3'\uparrow}^\dagger \\
&\quad \left. + \sqrt{6} \frac{c_{1\uparrow}^\dagger - c_{2\uparrow}^\dagger}{\sqrt{2}} \frac{c_{1'\downarrow}^\dagger c_{2'\uparrow}^\dagger c_{3'\uparrow}^\dagger + c_{1'\uparrow}^\dagger c_{2'\downarrow}^\dagger c_{3'\uparrow}^\dagger - c_{1'\uparrow}^\dagger c_{2'\uparrow}^\dagger c_{3'\downarrow}^\dagger}{\sqrt{3}} \right) |\Omega\rangle \\
H'|S = 0\rangle &= -\frac{t'}{6\sqrt{3}} \left( 2\sqrt{3} \frac{c_{1\uparrow}^\dagger - c_{2\uparrow}^\dagger}{\sqrt{2}} \frac{2c_{1'\downarrow}^\dagger c_{2'\downarrow}^\dagger c_{3'\uparrow}^\dagger - c_{1'\uparrow}^\dagger c_{2'\downarrow}^\dagger c_{3'\downarrow}^\dagger - c_{1'\downarrow}^\dagger c_{2'\uparrow}^\dagger c_{3'\downarrow}^\dagger}{\sqrt{3}} \right. \\
&\quad + 2\sqrt{3} \frac{c_{1\downarrow}^\dagger - c_{2\downarrow}^\dagger}{\sqrt{2}} \frac{2c_{1'\uparrow}^\dagger c_{2'\uparrow}^\dagger c_{3'\downarrow}^\dagger - c_{1'\uparrow}^\dagger c_{2'\downarrow}^\dagger c_{3'\uparrow}^\dagger - c_{1'\downarrow}^\dagger c_{2'\uparrow}^\dagger c_{3'\uparrow}^\dagger}{\sqrt{3}} \\
&\quad + 2\sqrt{3} \frac{c_{1\uparrow}^\dagger c_{2\downarrow}^\dagger c_{3\downarrow}^\dagger + c_{1\downarrow}^\dagger c_{2\uparrow}^\dagger c_{3\downarrow}^\dagger - 2c_{1\downarrow}^\dagger c_{2\downarrow}^\dagger c_{3\uparrow}^\dagger}{\sqrt{6}} \frac{c_{1'\uparrow}^\dagger - c_{2'\uparrow}^\dagger}{\sqrt{2}} \\
&\quad \left. + 2\sqrt{3} \frac{c_{1\downarrow}^\dagger c_{2\uparrow}^\dagger c_{3\uparrow}^\dagger + c_{1\uparrow}^\dagger c_{2\downarrow}^\dagger c_{3\uparrow}^\dagger - 2c_{1\uparrow}^\dagger c_{2\uparrow}^\dagger c_{3\downarrow}^\dagger}{\sqrt{6}} \frac{c_{1'\downarrow}^\dagger - c_{2'\downarrow}^\dagger}{\sqrt{2}} \right) |\Omega\rangle
\end{aligned} \tag{S7}$$

and with the results in SM. IB, the energy gain of different channels are

$$\Delta E^{(2)} = \begin{cases} -\frac{10t'^2}{27t} = J + \text{constant} & , S_{\text{tot}} = 2 \\ -\frac{6t'^2}{27t} = -J + \text{constant} & , S_{\text{tot}} = 1 \\ -\frac{4t'^2}{27t} = -2J + \text{constant} & , S_{\text{tot}} = 0 \end{cases} \tag{S8}$$

Noting here  $\frac{c_{1\uparrow}^\dagger - c_{2\uparrow}^\dagger}{\sqrt{2}} |\Omega\rangle$  and  $c_{1\uparrow}^\dagger c_{2\uparrow}^\dagger c_{3\uparrow}^\dagger |\Omega\rangle$  are all the eigen-state of intermediate states coincidentally, but in the following calculation, keeping in mind that before calculating the 2nd energy correction, make sure all intermediate states have been written into the linear combination of eigen-state of two trimers, which are all listed in SM. IB.

2. With flux  $\phi < \pi/2$

As all the preparation have been done in SM. IB, there only needs the calculation for intermediate states, which are written below

$$\begin{aligned}
H'|S=2\rangle &= \frac{t'}{3} \left[ (e^{-i\theta}c_{1\uparrow}^\dagger - e^{i\theta}c_{2\uparrow}^\dagger + 2i\sin\theta c_{3\uparrow}^\dagger)c_{1'\uparrow}^\dagger c_{2'\uparrow}^\dagger c_{3'\uparrow}^\dagger + 2\cos\theta c_{1\uparrow}^\dagger c_{2\uparrow}^\dagger c_{3\uparrow}^\dagger (c_{1'\downarrow}^\dagger - c_{2'\downarrow}^\dagger) \right] |\Omega\rangle \\
H'|S=1\rangle &= \frac{t'}{6} \left[ (e^{-i\theta}c_{1\uparrow}^\dagger - e^{i\theta}c_{2\uparrow}^\dagger + 2i\sin\theta c_{3\uparrow}^\dagger)(c_{1'\uparrow}^\dagger c_{2'\downarrow}^\dagger c_{3'\uparrow}^\dagger + c_{1'\downarrow}^\dagger c_{2'\uparrow}^\dagger c_{3'\uparrow}^\dagger - c_{1'\uparrow}^\dagger c_{2'\uparrow}^\dagger c_{3'\downarrow}^\dagger) \right. \\
&\quad - (e^{-i\theta}c_{1\downarrow}^\dagger - e^{i\theta}c_{2\downarrow}^\dagger + 2i\sin\theta c_{3\downarrow}^\dagger)c_{1'\uparrow}^\dagger c_{2'\uparrow}^\dagger c_{3'\uparrow}^\dagger \\
&\quad + 2\cos\theta c_{1\uparrow}^\dagger c_{2\uparrow}^\dagger c_{3\uparrow}^\dagger (c_{1'\downarrow}^\dagger - c_{2'\downarrow}^\dagger) \\
&\quad \left. + 2(-\sin\theta c_{1\uparrow}^\dagger c_{2\uparrow}^\dagger c_{3\downarrow}^\dagger + \sin\theta c_{1\downarrow}^\dagger c_{2\uparrow}^\dagger c_{3\uparrow}^\dagger - i\cos\theta c_{1\uparrow}^\dagger c_{2\uparrow}^\dagger c_{3\downarrow}^\dagger)(c_{1'\uparrow}^\dagger - c_{2'\uparrow}^\dagger) \right] |\Omega\rangle \\
H'|S=0\rangle &= \frac{t'}{6\sqrt{3}} \left[ (e^{-i\theta}c_{1\uparrow}^\dagger - e^{i\theta}c_{2\uparrow}^\dagger + 2i\sin\theta c_{3\uparrow}^\dagger)(2c_{1'\downarrow}^\dagger c_{2'\downarrow}^\dagger c_{2'\uparrow}^\dagger - c_{1'\uparrow}^\dagger c_{2'\uparrow}^\dagger c_{2'\downarrow}^\dagger - c_{1'\downarrow}^\dagger c_{2'\uparrow}^\dagger c_{2'\downarrow}^\dagger) \right. \\
&\quad + (e^{-i\theta}c_{1\downarrow}^\dagger - e^{i\theta}c_{2\downarrow}^\dagger + 2i\sin\theta c_{3\uparrow}^\dagger)(2c_{1'\uparrow}^\dagger c_{2'\uparrow}^\dagger c_{3'\downarrow}^\dagger - c_{1'\uparrow}^\dagger c_{2'\downarrow}^\dagger c_{3'\uparrow}^\dagger - c_{1'\downarrow}^\dagger c_{2'\uparrow}^\dagger c_{3'\uparrow}^\dagger) \\
&\quad + \left( (2e^{-i\theta} - e^{i\theta})c_{1\downarrow}^\dagger c_{2\uparrow}^\dagger c_{3\uparrow}^\dagger + (2e^{i\theta} - e^{-i\theta})c_{1\uparrow}^\dagger c_{2\downarrow}^\dagger c_{3\uparrow}^\dagger - 2\cos\theta c_{1\uparrow}^\dagger c_{2\uparrow}^\dagger c_{3\downarrow}^\dagger \right) (c_{1'\downarrow}^\dagger - c_{2'\downarrow}^\dagger) \\
&\quad \left. + \left( (2e^{-i\theta} - e^{i\theta})c_{1\uparrow}^\dagger c_{2\downarrow}^\dagger c_{3\downarrow}^\dagger + (2e^{i\theta} - e^{-i\theta})c_{1\downarrow}^\dagger c_{2\uparrow}^\dagger c_{3\downarrow}^\dagger - 2\cos\theta c_{1\downarrow}^\dagger c_{2\downarrow}^\dagger c_{3\uparrow}^\dagger \right) (c_{1'\uparrow}^\dagger - c_{2'\uparrow}^\dagger) \right] |\Omega\rangle
\end{aligned} \tag{S9}$$

and the corresponding energy gains are

$$\begin{aligned}
\Delta E_q^{(2)} &= -\frac{2t'^2}{9t} \left( \frac{\sin^2(\theta + \pi/6) + \cos^2\theta}{\sqrt{3}\cos(\theta - \pi/6)} + \frac{\sin^2(\theta - \pi/6) + \cos^2\theta}{\sqrt{3}\cos(\theta + \pi/6)} \right) \\
\Delta E_t^{(2)} &= -\frac{2t'^2}{9t} \left( \frac{\sin^2(\theta + \pi/6) + 1/2}{\sqrt{3}\cos(\theta - \pi/6)} + \frac{\sin^2(\theta - \pi/6) + 1/2}{\sqrt{3}\cos(\theta + \pi/6)} \right) \\
\Delta E_s^{(2)} &= -\frac{2t'^2}{9t} \left( \frac{\sin^2(\theta + \pi/6) + \frac{1}{4}(3 - 2\cos^2\theta)}{\sqrt{3}\cos(\theta - \pi/6)} + \frac{\sin^2(\theta - \pi/6) + \frac{1}{4}(3 - 2\cos^2\theta)}{\sqrt{3}\cos(\theta + \pi/6)} \right)
\end{aligned} \tag{S10}$$

The energy gains still satisfy the one of spin-1 Heisenberg model. The effective coupling with respect with flux  $\phi$  reads

$$\begin{aligned}
J(\phi) &= -\frac{t'^2}{18t} \frac{\cos\frac{2\phi}{3}\cos\frac{\phi}{3}}{\cos(\frac{\phi}{3} + \frac{\pi}{6})\cos(\frac{\phi}{3} - \frac{\pi}{6})} \\
&\approx J \left( 1 - \frac{7}{54}\phi^2 \right)
\end{aligned} \tag{S11}$$

which tells that the threading flux slightly weakens the FM channel, before  $\phi$  reaches  $\pi/2$ .

3. With flux  $\phi = \pi/2$

When  $\phi = \frac{\pi}{2}$ , in single trimer, singlet and triplet are both the GS, leading to extra channels between two trimers. For those channels between two trimers in triplet state, the energy gain can be spontaneously obtained by setting  $\phi = \pi/2$  according to Eq. (S10). What needs to be calculated only is the ones between trimers one/both of which is/are in singlet states, which is shown below:

$$\begin{aligned}
H'|k_0\rangle_A|k_{-1}\rangle_B &= \frac{t'}{3\sqrt{2}} \left[ (e^{-i\frac{\pi}{2}}c_{1\uparrow}^\dagger - e^{-i\frac{\pi}{6}}c_{2\uparrow}^\dagger + e^{i\frac{\pi}{6}}c_{3\uparrow}^\dagger)(c_{1'\uparrow}^\dagger c_{2'\downarrow}^\dagger c_{3'\uparrow}^\dagger - c_{1'\downarrow}^\dagger c_{2'\uparrow}^\dagger c_{3'\uparrow}^\dagger) \right. \\
&\quad - (c_{1\downarrow}^\dagger c_{2\uparrow}^\dagger c_{3\uparrow}^\dagger + e^{i\frac{\pi}{3}}c_{1\uparrow}^\dagger c_{2\downarrow}^\dagger c_{3\uparrow}^\dagger)(e^{i\frac{\pi}{6}}c_{1'\uparrow}^\dagger + e^{i\frac{7\pi}{6}}c_{2'\uparrow}^\dagger) \\
&\quad \left. + \sqrt{3}e^{i\frac{\pi}{6}}c_{1\uparrow}^\dagger c_{2\uparrow}^\dagger c_{3\uparrow}^\dagger (e^{i\frac{\pi}{6}}c_{1'\downarrow}^\dagger + e^{i\frac{7\pi}{6}}c_{2'\downarrow}^\dagger) \right] |\Omega\rangle \\
H'|k_{-1}\rangle_A|k_0\rangle_B &= \frac{t'}{3\sqrt{2}} \left[ (e^{-i\frac{\pi}{2}}c_{1\uparrow}^\dagger + e^{-i\frac{\pi}{6}}c_{2\uparrow}^\dagger + \sqrt{3}e^{i\frac{2\pi}{3}}c_{3\uparrow}^\dagger)c_{1'\uparrow}^\dagger c_{2'\uparrow}^\dagger c_{3'\downarrow}^\dagger \right. \\
&\quad - (e^{-i\frac{\pi}{2}}c_{1\downarrow}^\dagger + e^{-i\frac{\pi}{6}}c_{2\downarrow}^\dagger + \sqrt{3}e^{i\frac{2\pi}{3}}c_{3\downarrow}^\dagger)c_{1'\uparrow}^\dagger c_{2'\uparrow}^\dagger c_{3'\uparrow}^\dagger \\
&\quad \left. + (-e^{i\frac{\pi}{6}}c_{1\uparrow}^\dagger c_{2\uparrow}^\dagger c_{3\downarrow}^\dagger + e^{-i\frac{\pi}{6}}c_{1\uparrow}^\dagger c_{2\downarrow}^\dagger c_{3\uparrow}^\dagger + e^{i\frac{\pi}{2}}c_{1\downarrow}^\dagger c_{2\uparrow}^\dagger c_{3\uparrow}^\dagger)(c_{1'\uparrow}^\dagger - c_{2'\uparrow}^\dagger) \right] |\Omega\rangle \\
H'|k_{-1}\rangle_A|k_{-1}\rangle_B &= \frac{t'}{6} \left[ (e^{i\frac{\pi}{6}}c_{1\downarrow}^\dagger + e^{i\frac{\pi}{2}}c_{2\downarrow}^\dagger - \sqrt{3}e^{i\frac{\pi}{3}}c_{3\downarrow}^\dagger)(c_{1'\uparrow}^\dagger c_{2'\downarrow}^\dagger c_{3'\uparrow}^\dagger - c_{1'\downarrow}^\dagger c_{2'\uparrow}^\dagger c_{3'\uparrow}^\dagger) \right. \\
&\quad - (e^{i\frac{\pi}{6}}c_{1\uparrow}^\dagger + e^{i\frac{\pi}{2}}c_{2\uparrow}^\dagger - \sqrt{3}e^{i\frac{\pi}{3}}c_{3\uparrow}^\dagger)(c_{1'\uparrow}^\dagger c_{2'\downarrow}^\dagger c_{3'\downarrow}^\dagger - c_{1'\downarrow}^\dagger c_{2'\uparrow}^\dagger c_{3'\downarrow}^\dagger) \\
&\quad + (e^{-i\frac{\pi}{6}}c_{1\uparrow}^\dagger c_{2\downarrow}^\dagger c_{3\uparrow}^\dagger + e^{i\frac{\pi}{2}}c_{1\downarrow}^\dagger c_{2\uparrow}^\dagger c_{3\uparrow}^\dagger - e^{i\frac{\pi}{6}}c_{1\uparrow}^\dagger c_{2\uparrow}^\dagger c_{3\downarrow}^\dagger)(e^{i\frac{\pi}{3}}c_{1'\downarrow}^\dagger - c_{2'\downarrow}^\dagger) \\
&\quad \left. + (e^{-i\frac{\pi}{6}}c_{1\downarrow}^\dagger c_{2\uparrow}^\dagger c_{3\downarrow}^\dagger - e^{i\frac{\pi}{6}}c_{1\downarrow}^\dagger c_{2\downarrow}^\dagger c_{3\uparrow}^\dagger + e^{i\frac{\pi}{2}}c_{1\uparrow}^\dagger c_{2\downarrow}^\dagger c_{3\downarrow}^\dagger)(e^{i\frac{\pi}{3}}c_{1'\uparrow}^\dagger - c_{2'\uparrow}^\dagger) \right] |\Omega\rangle
\end{aligned} \tag{S12}$$

Unlike the former calculations, different channels are separated by symmetry, and the mixture between different channels is naturally forbidden. Here, according to the decomposition rule of the SU(2) representations, the two trimers have 6 spin channels, which are separated into three sectors. The quintet sector does not mix with others with the energy  $\Delta E_q^{(2)} = -\frac{2t'^2}{3\sqrt{3}t}$ . The two belonging to singlet sectors could mix with each other in principle, nevertheless, a straightforward calculation shows that the mixing matrix elements vanish at the 2nd order. The energies are simply the diagonal term  $\Delta E_{s,1}^{(2)} = -\frac{5t'^2}{12\sqrt{3}t}$  and  $\Delta E_{s,2}^{(2)} = -\frac{83t'^2}{108\sqrt{3}t}$ , which lies on the two ends of the energy spectrum. As for the three triplet sectors, their mixing matrix elements are calculated as:

$$H_{ab}^{(2)} = \sum_m \frac{\langle \psi_{a,s_z} | H' | m \rangle \langle m | H' | \psi_{b,s_z} \rangle}{E^{(0)} - E_m^{(0)}}, \tag{S13}$$

where  $a, b$  are the indices of sectors;  $s_z$  can take any value among  $\pm 1, 0$  yielding the same matrix elements according to the Wigner-Eckart theorem. Consequently, the secular equation reads

$$\Delta H_{S_{\text{tot}}=1}^{(2)} / \left( \frac{t'^2}{t} \right) = \begin{pmatrix} -\frac{1}{2\sqrt{3}} & -\frac{e^{i\pi/3}}{12\sqrt{6}} & 0 \\ -\frac{e^{-i\pi/3}}{12\sqrt{6}} & -\frac{7}{12\sqrt{3}} & 0 \\ 0 & 0 & -\frac{3}{4\sqrt{3}} \end{pmatrix} \tag{S14}$$

yielding the eigen-energies  $-\frac{13 \pm \sqrt{3}}{24\sqrt{3}} \frac{t'^2}{t}$  and  $-\frac{3}{4\sqrt{3}} \frac{t'^2}{t}$ . The above result shows when threading flux makes the singlet and triplet degenerate as ground-state, the system exhibit AFM rather than FM at the 2nd order, which seems to be 1st order phase transition.

## D. Phase transitions by tuning $t'$ and $U$

### 1. Competing between FM and AFM for finite $U$

In main content, we claim in our system, FM dominant because the intermediate states of FM are more coherent than the one of AFM. However this holds only for doubly occupancy states are projected because of infinite on-site interaction. In Fig 4(a) we observed that when  $t'/t = 0.2$ , FM occurs at  $U/t \approx 13 \sim 15$ , which tells when the interaction becomes finite, the occurrence of doubly occupancy leads to the competition between FM and AFM.

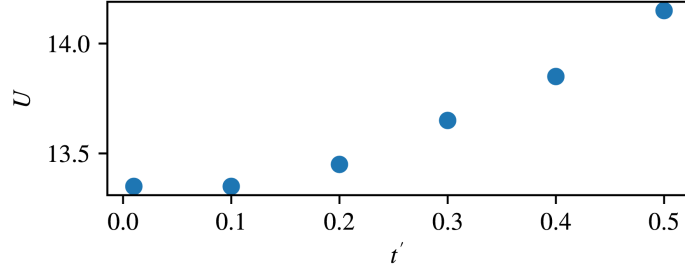


FIG. S2. Two-cluster estimation of spin exchange: The dependence of transition  $U$  between FM&AFM with respect to  $t'$ . Here  $t = 1$ .

Intermediate states contains double occupancy is shown below:

$$\begin{aligned}
H'|S=1\rangle &= \frac{t'}{6} \left[ (c_{1\uparrow}^\dagger - c_{2\uparrow}^\dagger)(-c_{1'\uparrow}^\dagger c_{2'\uparrow}^\dagger c_{3'\downarrow}^\dagger + c_{1'\uparrow}^\dagger c_{2'\downarrow}^\dagger c_{3'\uparrow}^\dagger + c_{1'\downarrow}^\dagger c_{2'\uparrow}^\dagger c_{3'\uparrow}^\dagger - 2c_{3'\uparrow}^\dagger c_{3'\downarrow}^\dagger c_{1'\uparrow}^\dagger - 2c_{3'\uparrow}^\dagger c_{3'\downarrow}^\dagger c_{2'\uparrow}^\dagger) \right. \\
&\quad - (c_{1\downarrow}^\dagger - c_{2\downarrow}^\dagger)c_{1'\uparrow}^\dagger c_{2'\uparrow}^\dagger c_{3'\uparrow}^\dagger + 2c_{1\uparrow}^\dagger c_{2\uparrow}^\dagger c_{3\uparrow}^\dagger (c_{1'\downarrow}^\dagger - c_{2'\downarrow}^\dagger) \\
&\quad \left. + 2(c_{1\uparrow}^\dagger c_{2\uparrow}^\dagger c_{3\downarrow}^\dagger - c_{1\uparrow}^\dagger c_{1\downarrow}^\dagger c_{2\uparrow}^\dagger - c_{2\uparrow}^\dagger c_{2\downarrow}^\dagger c_{3\uparrow}^\dagger + c_{1\uparrow}^\dagger c_{1\downarrow}^\dagger c_{3\uparrow}^\dagger + c_{2\uparrow}^\dagger c_{2\downarrow}^\dagger c_{1\uparrow}^\dagger)(c_{1'\uparrow}^\dagger - c_{2'\uparrow}^\dagger) \right] |\Omega\rangle \\
H'|S=0\rangle &= \frac{t'}{6\sqrt{3}} \left[ (c_{1\uparrow}^\dagger - c_{2\uparrow}^\dagger)(2c_{1'\downarrow}^\dagger c_{2'\downarrow}^\dagger c_{3'\uparrow}^\dagger - c_{1'\downarrow}^\dagger c_{2'\uparrow}^\dagger c_{3'\downarrow}^\dagger - c_{1'\uparrow}^\dagger c_{2'\downarrow}^\dagger c_{3'\downarrow}^\dagger + 3c_{3'\uparrow}^\dagger c_{3'\downarrow}^\dagger c_{1'\downarrow}^\dagger - 3c_{3'\uparrow}^\dagger c_{3'\downarrow}^\dagger c_{2'\downarrow}^\dagger) \right. \\
&\quad + (c_{1\downarrow}^\dagger - c_{2\downarrow}^\dagger)(2c_{1'\uparrow}^\dagger c_{2'\uparrow}^\dagger c_{3'\downarrow}^\dagger - c_{1'\uparrow}^\dagger c_{2'\downarrow}^\dagger c_{3'\uparrow}^\dagger - c_{1'\downarrow}^\dagger c_{2'\uparrow}^\dagger c_{3'\uparrow}^\dagger - 3c_{3'\uparrow}^\dagger c_{3'\downarrow}^\dagger c_{1'\uparrow}^\dagger + 3c_{3'\uparrow}^\dagger c_{3'\downarrow}^\dagger c_{2'\uparrow}^\dagger) \\
&\quad + (-2c_{1\uparrow}^\dagger c_{2\uparrow}^\dagger c_{3\downarrow}^\dagger + c_{1\uparrow}^\dagger c_{2\downarrow}^\dagger c_{3\uparrow}^\dagger + c_{1\downarrow}^\dagger c_{2\uparrow}^\dagger c_{3\uparrow}^\dagger - 3c_{1\uparrow}^\dagger c_{1\downarrow}^\dagger c_{2\uparrow}^\dagger - 3c_{2\uparrow}^\dagger c_{2\downarrow}^\dagger c_{3\uparrow}^\dagger + 3c_{1\uparrow}^\dagger c_{1\downarrow}^\dagger c_{3\uparrow}^\dagger + 3c_{2\uparrow}^\dagger c_{2\downarrow}^\dagger c_{1\uparrow}^\dagger)(c_{1'\downarrow}^\dagger - c_{2'\downarrow}^\dagger) \\
&\quad \left. + (-2c_{1\downarrow}^\dagger c_{2\downarrow}^\dagger c_{3\uparrow}^\dagger + c_{1\downarrow}^\dagger c_{2\uparrow}^\dagger c_{3\downarrow}^\dagger + c_{1\uparrow}^\dagger c_{2\downarrow}^\dagger c_{3\downarrow}^\dagger + 3c_{1\uparrow}^\dagger c_{1\downarrow}^\dagger c_{2\downarrow}^\dagger + 3c_{2\uparrow}^\dagger c_{2\downarrow}^\dagger c_{3\downarrow}^\dagger - 3c_{1\uparrow}^\dagger c_{1\downarrow}^\dagger c_{3\downarrow}^\dagger - 3c_{2\uparrow}^\dagger c_{2\downarrow}^\dagger c_{1\downarrow}^\dagger)(c_{1'\uparrow}^\dagger - c_{2'\uparrow}^\dagger) \right] \tag{S15}
\end{aligned}$$

where we ignore the calculation of state  $|S=2\rangle$  because in fully polarized state, doubly occupancy states are forbidden by Pauli exclusion principle. The calculation shows the corresponding energy gains are

$$\begin{aligned}
\Delta E_q^{(2)} &= -\frac{10t'^2}{27t} \\
\Delta E_t^{(2)} &= -\left(\frac{6t'^2}{27t} + \frac{124t'^2}{81U}\right) \\
\Delta E_s^{(2)} &= -\left(\frac{4t'^2}{27t} + \frac{186t'^2}{81U}\right)
\end{aligned} \tag{S16}$$

which yields a full super-exchange coupling

$$J = -\frac{2t'^2}{27t} + \frac{62t'^2}{81U} \tag{S17}$$

The opposite sign of  $t$ - and  $U$ -term illustrates the competition between FM&AFM.

A numerical result with exact diagonalization (ED) is also obtained, about the dependence of critical transition interaction  $U_c$  with respect with  $t'$ , as depicted in Fig. S2. It shows that when  $t'/t$  is larger than 0.2, it generates more high-order super-exchange process, which strengthens AFM phase. Rather, if  $t'/t$  is small, the critical  $U$  tends to the value 13.35, which is also at the level of  $U/t \sim 10$ .

## 2. Competing between FM and AFM for finite $U$ in trimerized Kagome lattice

A similar calculation is easily generalized to Kagome lattice. First, the Bloch Hamiltonian for trimerized Kagome lattice is

$$\begin{pmatrix}
0 & t + t'e^{-i\vec{k}\cdot\vec{a}_1} & t + t'e^{-i\vec{k}\cdot\vec{a}_2} \\
t + t'e^{i\vec{k}\cdot\vec{a}_1} & 0 & t + t'e^{-i\vec{k}\cdot(\vec{a}_1+\vec{a}_2)} \\
t + t'e^{i\vec{k}\cdot\vec{a}_2} & t + t'e^{i\vec{k}\cdot(\vec{a}_1+\vec{a}_2)} & 0
\end{pmatrix} \tag{S18}$$

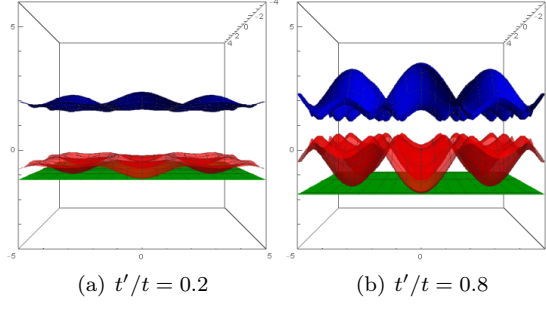


FIG. S3. The free band structure of trimerized Kagome lattice with respect to ratio  $t'/t$ .

where  $\vec{k} = (k_x, k_y)$  and  $\vec{a}_1 = (2, 0)$ ,  $\vec{a}_2 = (1, \sqrt{3})$ . Different from the trimerized triangular lattice, due to the existence of one flat band, the energy bands are written as a simple form, which reads:

$$\begin{aligned} \varepsilon_1 &= -(t + t') \\ \varepsilon_{2,3} &= \frac{t + t'}{2} \pm \frac{1}{2} \sqrt{9t^2 + 9t'^2 + 2(4K - 3)tt'} \end{aligned} \quad (\text{S19})$$

where  $K = \cos[\vec{k} \cdot (\vec{a}_1 - \vec{a}_2)] + \cos \vec{k} \cdot \vec{a}_2 + \cos \vec{k} \cdot \vec{a}_1$ , and they are shown in Fig. S3. The flat band structure is robust regardless of  $t'$ , up to an energy shift.

Second, the intermediate states calculations are

$$\begin{aligned} H'|S=2\rangle &= \frac{t'}{3} \left[ (c_{3\uparrow}^\dagger - c_{2\uparrow}^\dagger)c_{1'\uparrow}^\dagger c_{2'\uparrow}^\dagger c_{3'\uparrow}^\dagger + c_{1\uparrow}^\dagger c_{2\uparrow}^\dagger c_{3\uparrow}^\dagger (c_{1'\uparrow}^\dagger - c_{2'\uparrow}^\dagger) \right] |\Omega\rangle \\ H'|S=1\rangle &= \frac{t'}{6} \left[ (c_{3\uparrow}^\dagger - c_{2\uparrow}^\dagger)(-c_{1'\uparrow}^\dagger c_{2'\uparrow}^\dagger c_{3'\downarrow}^\dagger + c_{1'\uparrow}^\dagger c_{2'\downarrow}^\dagger c_{3'\uparrow}^\dagger + c_{1'\downarrow}^\dagger c_{2'\uparrow}^\dagger c_{3'\uparrow}^\dagger - 2c_{3'\uparrow}^\dagger c_{3'\downarrow}^\dagger c_{1'\uparrow}^\dagger - 2c_{3'\uparrow}^\dagger c_{3'\downarrow}^\dagger c_{2'\uparrow}^\dagger) \right. \\ &\quad - (c_{1\downarrow}^\dagger - c_{2\downarrow}^\dagger)c_{1'\uparrow}^\dagger c_{2'\uparrow}^\dagger c_{3'\uparrow}^\dagger + c_{1\uparrow}^\dagger c_{2\uparrow}^\dagger c_{3\uparrow}^\dagger (c_{1'\downarrow}^\dagger - c_{2'\downarrow}^\dagger) \\ &\quad \left. + (c_{1\downarrow}^\dagger c_{2\uparrow}^\dagger c_{3\uparrow}^\dagger - c_{1\uparrow}^\dagger c_{2\uparrow}^\dagger c_{3\downarrow}^\dagger - c_{1\uparrow}^\dagger c_{2\downarrow}^\dagger c_{3\uparrow}^\dagger - 2c_{1\uparrow}^\dagger c_{1\downarrow}^\dagger c_{2\uparrow}^\dagger + 2c_{1\uparrow}^\dagger c_{1\downarrow}^\dagger c_{3\uparrow}^\dagger)(c_{1'\uparrow}^\dagger - c_{2'\uparrow}^\dagger) \right] |\Omega\rangle \\ H'|S=0\rangle &= \frac{t'}{6\sqrt{3}} \left[ (c_{3\uparrow}^\dagger - c_{2\uparrow}^\dagger)(2c_{1'\downarrow}^\dagger c_{2'\downarrow}^\dagger c_{3'\uparrow}^\dagger - c_{1'\uparrow}^\dagger c_{2'\downarrow}^\dagger c_{3'\downarrow}^\dagger - c_{1'\downarrow}^\dagger c_{2'\uparrow}^\dagger c_{3'\downarrow}^\dagger) \right. \\ &\quad + (c_{3\downarrow}^\dagger - c_{2\downarrow}^\dagger)(2c_{1'\uparrow}^\dagger c_{2'\uparrow}^\dagger c_{3'\downarrow}^\dagger - c_{1'\uparrow}^\dagger c_{2'\downarrow}^\dagger c_{3'\uparrow}^\dagger - c_{1'\downarrow}^\dagger c_{2'\uparrow}^\dagger c_{3'\uparrow}^\dagger) \\ &\quad + (2c_{1\downarrow}^\dagger c_{2\uparrow}^\dagger c_{3\uparrow}^\dagger - c_{1\uparrow}^\dagger c_{2\uparrow}^\dagger c_{3\downarrow}^\dagger - c_{1\uparrow}^\dagger c_{2\downarrow}^\dagger c_{3\uparrow}^\dagger)(c_{1'\downarrow}^\dagger - c_{2'\downarrow}^\dagger) \\ &\quad \left. + (2c_{1\uparrow}^\dagger c_{2\downarrow}^\dagger c_{3\downarrow}^\dagger - c_{1\downarrow}^\dagger c_{2\uparrow}^\dagger c_{3\downarrow}^\dagger - c_{1\downarrow}^\dagger c_{2\downarrow}^\dagger c_{3\uparrow}^\dagger)(c_{1'\uparrow}^\dagger - c_{2'\uparrow}^\dagger) \right] |\Omega\rangle \end{aligned} \quad (\text{S20})$$

which generates the energy gains are

$$\begin{aligned} \Delta E_q^{(2)} &= -\frac{2t'^2}{27t} \\ \Delta E_t^{(2)} &= -\left( \frac{2t'^2}{27t} + \frac{88t'^2}{81U} \right) \\ \Delta E_s^{(2)} &= -\left( \frac{2t'^2}{27t} + \frac{44t'^2}{27U} \right) \end{aligned} \quad (\text{S21})$$

The effective coupling is

$$J = \frac{44t'^2}{81U} \quad (\text{S22})$$

which is AFM one at all time. The physical picture of the difference between trimerized Kagome lattice and trimerized triangular lattice is given in main context.